ILMATIETEEN LAITOS
METEOROLOGISKA INSTITUTET
FINNISH METEOROLOGICAL INSTITUTE

RAPORTTEJA
RAPPORTER
REPORTS
2017:2

METHOD FOR CONSTRUCTING AN AOD-RELATED ATMOSPHERIC CORRECTION TIME SERIES FOR THE CLARA-A2 SAL DATA RECORD

EMMIHENNA JÄÄSKELÄINEN
TERHIKKI MANNINEN
JOHANNA TAMMINEN
MARKO LAINE

WWW.FMI.FI

FINNISH METEOROLOGICAL INSTITUTE

Published by	Finnish Meteorological Institute (Erik Palménin aukio 1) , P.O. Box 503 FIN-00101 Helsinki, Finland	Series title, number and report code of publication Reports 2017:2 Date September 2017
Author(s)	Emmihenna Jääskeläinen, Terhikki Manninen, Johanna Tamminen and Marko Laine	Name of project Commissioned by
Title	Method for constructing an AOD-related atmospheric correction time series for the CLARA-A2 SAL data record	

Abstract

In the Satellite Application Facility on Climate Monitoring (CM SAF) project, financially supported by EUMETSAT, the 34-year long (1982-2015) broadband albedo time series CLARA-A2 SAL (the Surface ALbedo from the CM SAF cLoud, Albedo and RAdiation data record, second version) was produced from Advanced Very High Resolution Radiometer (AVHRR) measurements. CLARA-A2 SAL data record uses a Simplified Method for Atmospheric Correction algorithm SMAC for correcting for atmospheric effects. Aerosol optical depth (AOD) is the main input of the algorithm. Because there were no global AOD time series for the whole needed time period (1982-2015), the AOD-related time series were constructed, and the method for calculating it is described in this report.

Publishing unit: Meteorological research

Classification (UDC)	Keywords: aod, ai, aerosol optical depth, aerosol index, atmospheric correction, smac,
ISSN and series title 0782-6079 Raportteja – Rapporter - Reports	
ISBN: 978-952-336-013-6 (pdf)	Language: English Pages: 24

Method for constructing an AOD-related atmospheric correction time series for the CLARA-A2 SAL data record

Emmihenna Jääskeläinen, Terhikki Manninen, Johanna Tamminen, Marko Laine

September 19, 2017

1 Introduction

In the Satellite Application Facility on Climate Monitoring (CM SAF, `http://www.cmsaf.eu/EN/Home/home_node.html`) project, financially supported by EUMETSAT, the 34-year long (1982–2015) broadband albedo time series CLARA-A2 SAL (the Surface ALbedo from the CM SAF cLoud, Albedo and RAdiation data record, second version) was produced from Advanced Very High Resolution Radiometer (AVHRR) measurements. Its predecessor, CLARA-A1 SAL, covered the years 1982–2009.

Both data records use a Simplified Method for Atmospheric Correction algorithm SMAC [1] for correcting for atmospheric effects. Aerosol optical depth (AOD) is the main input of the algorithm, and for the CLARA-A1 SAL data record it was fixed to have a constant value 0.1, because there were no global AOD time series for the whole needed time period. For the CLARA-A2 SAL data record, the needed AOD-related time series were constructed, and the method for calculating it is described in this report.

The AOD-related time series are constructed from aerosol index (AI) at UV-wavelength range from Total Ozone Mapping Spectrometer (TOMS) and Ozone Monitoring Instrument (OMI) together with the Solar Zenith Angle (SZA) and land use classification (LUC) information. The regression formulas are statistical, rather than based directly on any physical relationship. Some attempts to construct AOD from AI have been made [2, 3], but there are no daily AOD data with the global coverage needed for more accurate albedo information. The aerosol information is calculated from the AI data for the period 1982–2014, and for the year 2015 the AOD data are a climatology of the calculated aerosol values from the years 2005–2014, because the quality of the AI data deteriorated seriously in 2015.

The AI data were chosen, because there are no other aerosol-related data than AI for the whole needed period (1982–2015). AI is dependent on AOD, on the height of the aerosol layer, on the absorption properties of aerosols [4], and also on the surface albedo, on the solar and viewing geometry, and on the used wavelength pair [5]. There are no global data for the height of the aerosol layer or other quantities which could be used in the process of constructing AOD time series for the whole time period 1982–2014, only the AI data. Estimating AOD of scattering aerosols at 550 nm using the UV information is justified, because the wavelength difference is relatively small to allow using the Ångström exponent relation. For absorbing aerosols one cannot expect to get a direct relationship between two wavelengths. In that case the statistical relationship between the amounts of scattering and absorbing aerosols seems to be typically strong enough to provide good-enough results. The SMAC algorithm is not developed to cope with AOD values higher than unity and the CLARA-A2 SAL algorithm uses only the pixels for which the SZA is below 70°, so the AOD-related time series have those advantages.

In this method, AI data are used as a proxy for the total column AOD everywhere, even though the AI is

only largely sensitive to smoke, desert dust and volcanic ash [6]. This conscious choice is due to the lack of any other usable data for the whole needed period 1982–2014. The quality of this approach is checked using existing AOD data retrievals.

This report is organized as follows. In Section 2 we present the data used in this method, and it is followed by Section 3 where we describe the method for the time series construction. In Section 4 we describe the calculation of the AOD time series from TOMS-AI and OMI-AI.

2 Data

The properties of the instruments, which data we used for constructing the time series, are presented in Table 1.

2.1 Data sources

TOMS instruments, observing AI, have been aboard Nimbus-7, Meteor-3, Earth Probe and ADEOS satellites, but only the AI retrievals from Nimbus-7 (TOMSN7L3, [7]) and Earth Probe (TOMSEPL3, [8]) are used for time series construction (Subsection 4.2). Nimbus-7 TOMS provide global daily coverage of Level-3 AI data from 1978 to mid-1993. Earth Probe TOMS and ADEOS TOMS made the measurements at the same time, but the Earth Probe was placed into a lower orbit than ADEOS resulting in finer spatial resolution at the expense of full global coverage. When ADEOS stopped service in December 1997, the Earth Probe was boosted to a higher orbit enabling geographically larger daily coverage. The AI data from Earth Probe are from mid-1996 to 2005. [9, 10]

The OMI instrument aboard Aura satellite provides global daily AI and AOD data from the late 2004 onwards. The measurements are made in the afternoon local time. The OMI observations suffer from a row anomaly problem since 2009. It varies with time and it affects the quality of the Level-1b radiance, and consequently Level-2, data products. Level-3 data, which is used in the time series construction, are produced from filtered Level-2 data [11]. AI and AOD data (OMAEROe, [12]) from the years 2005–2010 are used for the best-fitting-function method (Section 3) and AI data from the years 2005–2014 are used as an input data for the AOD time series construction (Subsection 4.1).

The MODerate resolution Imaging Spectroradiometer (MODIS), aboard the Earth Observation System's (EOS) Terra and Aqua satellites, is used for retrieval of AOD. Terra is on a descending orbit (southward) over the equator and AOD retrievals are made around 10:30 local solar time. Aqua is on an ascending orbit (northward) over the equator and AOD retrievals are made around 13:30 local solar time. [13] The MODIS-Aqua AOD data are used for cloud-screening (Subsection 3.2), because it is closer in time with OMI measurements. The MODIS-AOD data from Collection 005 are used instead of Collection 006, because Collection 006 were unavailable at the time the correction data set was generated. The AOD data we used (MYD08 product) are Level-3 data from the Dark Target [14, 15, 16, 17] and Deep Blue [18, 19] algorithms.

The AVHRR Land Use Classification (LUC) data [20] was generated in 1998 using AVHRR imagery for years 1981–1994. This AVHRR-LUC data is chosen because the CLARA-A2 SAL time series is calculated from the AVHRR data. In this study we used the LUC map with spatial resolution of 1° for the subclass division (Subsection 3.2). These subclasses are used to provide opportunities for regional inspections, especially when AOD values are related to some special land cover classes and locations. AVHRR-LUC provides accurate land use classification on land, but it is too coarse for coastal areas ($1^\circ \times 1^\circ$ compared to the used

OMI resolution $0.25^\circ \times 0.25^\circ$). Global Land Cover 2000 (GLC2000) provides finer spatial resolution data, $0.01^\circ \times 0.01^\circ$ [21], and it is used to refine the coastal areas (Subsection 3.2).

2.2 Data description

The aerosol index is defined as

$$\mathrm{AI} = -100 \cdot \left\{ \log_{10}\left[\left(\frac{I_{\lambda_1}}{I_{\lambda_2}}\right)_M\right] - \log_{10}\left[\left(\frac{I_{\lambda_1}}{I_{\lambda_2}}\right)_C\right] \right\} \tag{1}$$

where $I_{\lambda_1 M}$ and $I_{\lambda_2 M}$ are the radiances measured by instrument M at wavelengths λ_1 and λ_2, and $I_{\lambda_1 C}$ and $I_{\lambda_2 C}$ are the calculated radiances, which are produced by a radiative transfer model for a pure Rayleigh atmosphere [6], [4]. The used wavelengths for AI calculation are 331–360 nm (TOMS) and 354–388 nm (OMI).

The OMTO3d data set [22], where AI is calculated using the same wavelengths and the same algorithm (v8) as the TOMS-AI from Nimbus-7 and Earth Probe, would be a more logical AI data set instead of OMAEROe AI. But despite homogeneous AI data, the OMAEROe AI data is closer with the TOMS-AI data, which can be seen from Figure 1. We compared globally TOMS-AI from the year 2000 with Terra MODIS-AOD from the same year (black), and we also compared OMAEROe-AI (blue) and OMTO3d-AI (red) data from the year 2005 to the Terra MODIS-AOD data from the year 2005. It shows that if we assume that Terra MODIS-AOD from the years 2000 and 2005 behave similarly, the OMAEROe-AI is actually closer with the TOMS-AI than the OMTO3d-AI data, at least when AOD is limited to the range [0,1]. The upper limit of the reddish (or blueish) area behind the curves indicates the mean of OMAEROe-AI (OMTO3d-AI) values with added standard deviation and the lower limit indicates the mean of OMAEROe-AI (OMTO3d-AI) values with subtracted standard deviation. To justify the assumption of similar MODIS-AOD data between years 2000 and 2005, we inspected the zonal daily means of absolute differences between the AOD data from both of these years. The zonal means are in Figure 2 and the corresponding standard deviations are in Figure 3. There are some days where the zonal means of the absolute differences are clearly high, over the range [-0.4, 0.4], but mostly they are around zero.

The TOMS data contains only positive AI values (absorbing aerosols) whereas OMI data include also negative AI values (non-absorbing aerosols). To keep the time series input data homogeneous, we use only positive AI values. This means that approximately 30–40% of OMI-AI values are discarded (a minimum of 25% at the start of the year and a maximum of 40% around July every year). The discarded data are typically from sea-salt particles and sulphate aerosols. The geographic location of negative AI values in percentages in 2008 are shown in Figure 4. In the other years (2005–2007, 2009–2014) the data show a similar kind of behaviour. Figure 4 shows that no areas are completely covered by negative AI values ensuring that all areas have at least some positive AI values. And even though through rejecting negative AI values a part of the aerosol information are excluded, some of that information is implicitly included in the AOD time series construction by using total AOD values for comparisons with AI instead of only using absorbing AOD values together with land use classification information.

Aerosol optical depth is defined as

$$\tau(\lambda) = \int_0^{\mathrm{TOA}} k_{\mathrm{ext}}(\lambda, z)\,\mathrm{d}z \tag{2}$$

where $\tau(\lambda)$ is AOD at wavelength λ , k_{ext} is the wavelength depending on the aerosol extinction coefficient, which is a measure of the attenuation of the incoming solar radiation by particle scattering k_{sca} and absorption k_{abs}, i.e. $k_{\mathrm{ext}} = k_{\mathrm{sca}} + k_{\mathrm{abs}}$ [23]. Thus, AOD is the aerosol extinction coefficient vertically integrated from the surface to the top of the atmosphere. In this study we are using the OMAEROe product, where AOD values are retrieved using a Multi-wavelength method instead of OMAERUVd product, where the AOD are retrieved using a Near-UV method [23].

3 The process

The AOD calculation method is based on Level-3 data of AI and AOD from the OMI instrument from the years 2005–2010. The data from the years 2005–2008 are used for constructing the regression functions and the data from the years 2009–2010 are used to choose the best functions for each subclass.

3.1 Limitations

1. AOD < 1;
2. SZA $< 70^\circ$;
3. AOD values are constructed only for land;
4. Only positive AI values are used.

3.2 Preprocessing and prerequisites

1. World map division and coastal refinement
   - **What:** Dividing the world map into the 65 subclasses on the basis of the AVHRR Land Use Classification map and refining the coastal areas by using GLC2000 data.
   - **Why:** Some land cover classes are related to certain AOD values, and hence the subclass division adds geophysical information to the time series construction. The coastal refinement is needed, because AVHRR-LUC is too coarse in those areas ($1^\circ \times 1^\circ$ compared to the used OMI resolution $0.25^\circ \times 0.25^\circ$).
   - **How:** Each land use class from AVHRR-LUC is manually divided into 2 or more subclasses based on how close the pixels are located to each other. An example of subclass division is in Figure 5, and more details about the land use classes are provided in Tables 2 - 4. For the coastal refinement, we use a water mask of $0.25^\circ \times 0.25^\circ$ resolution, constructed from the GLC2000 data (resolution of $0.01^\circ \times 0.01^\circ$), where a pixel is marked as water if all the smaller pixels are marked as such.
2. Calculation of OMI-AOD at the 550 nm wavelength
   - **What:** Estimation of OMI-AOD at the 550 nm wavelength.
   - **Why:** The SMAC algorithm needs the AOD values at 550 nm, and the used OMAEROe product contains only the AOD values at the wavelengths 342.5 nm, 388 nm, 442 nm, 463 nm and 483.5 nm.
   - **How:** The AOD at the 550 nm is calculated using the formula [24]

$$\tau_{550} = \tau_{\lambda_{UV}} \cdot \left(\frac{550}{\lambda_{UV}} \right)^{-\alpha} \tag{3}$$

   where τ_{550} is the AOD value at 550 nm, $\tau_{\lambda_{UV}}$ is the AOD value at the wavelength λ_{UV} and the exponent α is the Ångström exponent. The AOD at the 550 nm wavelength is estimated once from each reported wavelength pair and the used Ångström exponent is calculated from those wavelengths in question. The final OMI-AOD at 550 nm is the mean value of all the estimates, and it is marked τ_{550} from now on.

3. Screening the data

   - **What:** Screening the τ_{550} and the corresponding OMI-AI data for clouds, and masking away the unusable data.

   - **Why:** Cloud-screening the OMI data is necessary, because partly cloudy pixels are not always recognized and that may cause an overestimation of the AOD values [25]. The unusable data is masked to homogenize the OMI-AI data levels with TOMS-AI data levels and to specify the data for the SMAC algorithm (AOD below unity and SZA below 70°).

   - **How:** The τ_{550} and the corresponding OMI-AI data are cloud-screened by using the cloud-free MODIS-AOD Level-3 data. The MODIS-AOD pixels ($1^\circ \times 1^\circ$ resolution) are first resampled to the OMI resolution ($0.25^\circ \times 0.25^\circ$) and then the AOD data sets are compared pixelwise. The AOD pixels (and the corresponding AI pixels), for which the relative difference exceeds 20%, are masked. To homogenize the OMI-AI data levels with the TOMS-AI data levels, the OMI-AI values lesser than 0.5, or greater than 4.5, are masked also (with corresponding τ_{550} values). Also, the atmospheric correction algorithm SMAC is not developed to handle with AOD values higher than unity and the CLARA-A2 SAL algorithm uses only the pixels for which SZA is smaller than 70°, so those pixels which do not satisfy these restrictions are masked too.

4. Subclass correlations 2005–2008

   - **What:** Calculation of correlation coefficients between τ_{550} and OMI-AI, between τ_{550} and SZA, and between τ_{550} and $\mathrm{AI}\cdot\cos(\theta)$ (where θ is the SZA in radiances) for each subclass for the years 2005–2008 (Figure 6).

   - **Why:** To see how good the relationships between τ_{550} and AI data are, and whether including SZA information improves the results.

   - **Results:** The correlation between τ_{550} and OMI-AI is mainly around 0.3, but the variation is large (the topmost figure from Figure 6). The correlation coefficients between τ_{550} and SZA (the middle figure) vary less, but the values are mainly lower, around 0.2. The coefficients are improved slightly when combining the AI with the SZA information (the bottom figure) and the values range from around 0.3 to 0.6. The subclass 20 (part of southern Chile) appears to be problematic, the coefficients are low in every scenario. It is likely due to the inhomogeneous geography and small number of pixels (309 pixels from 2005–2008 with a minimum 27 in subclass 27 and a maximum 1737422 in subclass 39) in this subclass.

5. Pixelwise correlations 2005–2008

   - **What:** Calculation of the pixelwise correlation coefficients between τ_{550} and $\mathrm{AI}\cdot\cos(\theta)$ (where θ is the SZA in radiances) for the years 2005-2008 (Figure 7). Only those pixels which have more than 2 values are included.

   - **Why:** To see the relationship between τ_{550} and AI data globally over four years.

   - **Results:** The correlation coefficients are mainly around 0.5 or larger than that in many areas like the Amazon, the Sahara, the Middle East and Australia. The combined results from Figures 6 and 7 support the idea of constructing the AOD-related time series from OMI-AI together with SZA and land use classification information.

3.3 Method

The flowchart of the method is shown in Figure 8.

1. Deseasonalization

   - **What:** Deseasonalizing the preprocessed τ_{550} and OMI-AI data.
   - **Why:** Deseasonalization is made to remove the annual variation while leaving the trend in the data and hence providing an independent relationship between τ_{550} and OMI-AI. The seasonality is imported back into the data during the time series calculation process (Section 4).
   - **How:** Deseasonalization is made separately for each subclass using the formula

   $$z_i = y_i - (y_{mm_i} - y_{a_i}) \tag{4}$$

   where i is the index of the subclass ($i \in [1,65]$); y_i is the original value of the pixel in the subclass i; y_{mm_i} is the monthly mean (or monthly median) of the subclass i; y_{a_i} is the annual mean (or annual median) of the subclass i, and z_i is the deseasonalized value of the pixel in the subclass i. The coefficients y_{mm_i} and y_{a_i} are calculated as adaptive, geographically weighted averages and medians. Two approaches (mean and median) offer two slightly different data sets and hence provide more alternatives for the time series calculation.

   The data (τ_{550} and OMI-AI) in each subclass are divided into bins with a length of 0.1.

   – **Weighted average:** To obtain the weights, the bins are ordered by the number of values in each bin. The weight is determined to be the number of the ordered bin divided by the total number of bins (for example the value belonging to the bin with the largest number of counts receives the highest weight).

   – **Weighted median:** A vector is constructed by adding each value to the vector as many times as the number of the values in the bin in which the value belongs to is, and then the median is calculated from the vector.

2. Regression computation

   - **What:** Calculations of the pixelwise regressions between τ_{550} and OMI-AI data (together with SZA information), which are deseasonalized using weighted mean coefficients (marked as data set D_{mean}), and pixelwise regressions between τ_{550} and OMI-AI data (together with SZA information), which are deseasonalized using weighted median coefficients (marked as data set D_{median}).
   - **Why:** The pixelwise regressions allow more variability in the values.
   - **How:** The linear regression functions, for the AOD at 550 nm wavelength, have the form

   $$\widetilde{\tau} = \alpha \cdot \widetilde{AI} \cdot \cos(\theta) + \beta \tag{5}$$

   where $\widetilde{\tau}$ and $\widetilde{AI}$ denote modified (preprocessed and deseasonalized) AOD and AI data, respectively, and θ is SZA. Other models were also studied, but they are not shown here. The chosen model is the simplest one from the ones that performed best when taking into consideration the SZA dependence in the AOD data and independence in the AI data.

3. Forming subclass functions

   - **What:** Constructing eight (8) possible functions for each subclass.

- **Why:** To allow different kind of scenarios for diverse subclasses.

- **How:** By applying the pixelwise regression functions to both data sets (D_{mean}, D_{med}) we calculate the AOD estimates for the years 2005–2008. The calculated AOD estimates are then compared to the τ_{550} values within each subclass through pixelwise correlations. We calculate the median of those regression coefficients (α, β) that have a correlation coefficient r higher or equal to 0.5. In the same way we calculate the median of those regression coefficients which have a correlation coefficient $r \geq 0.6$, $r \geq 0.7$ and $r \geq 0.8$. These calculated median α and β values are used as possible function coefficients to be tested.

4. Choosing the best function for each subclass

   - **What:** We choose the best functions from the eight possible ones (the forms of the functions are in flowchart in Figure 8) for each subclass to use in the time series calculation by calculating the AOD estimates for the years 2009–2010 using these functions.

   - **Why:** The data from the years 2009–2010 were not included in the regression parameter retrieval.

   - **How:** First we homogenize the OMI-AI data levels (from the years 2009–2010) with TOMS data levels to achieve data that are as well inter-calibrated as possible. We average the OMI-AI data to the TOMS-AI resolution ($1^\circ \times 1.25^\circ$) with restrictions $0.5 \leq \mathrm{AI} \leq 4.5$ and then we resample the data to the original OMI resolution ($0.25^\circ \times 0.25^\circ$). Then the AI data is deseasonalized (as described in step 1 in the Methods) with the deseasonalization coefficients calculated by using the homogenized data from the years 2009–2010. After that the AOD values are calculated by using the eight possible functions, and the resulting τ_{calc} values are compared to the τ_{550} values. For each subclass, the function which yields the smallest absolute difference is chosen. The chosen functions are presented in Table 5, where D stands for which deseasonalization method (mean or median) is used and r stands for the correlation coefficient value that was used for determining the regression function coefficients for the subclass.

4 The AOD time series calculation

The flowchart of the process is shown in Figure 9.

4.1 AOD from the OMI-AI

1. **Homogenization and deseasonalization.** We have OMI-AI data for the years 2005–2014. The AI data are not preprocessed to the same extent as the AI data for the best-function calculation process. The used data is only homogenized with the TOMS data, and the AI values which are either below 0.5 or above 4.5 are discarded. Then the AI data are deseasonalized (the same way as described in step 1 in the Methods) with the deseasonalization coefficients calculated by using the homogenized data from the years 2005–2014.

2. **AOD calculation.** The data screening may cause gaps in daily AI maps. We try to fill the missing pixels by using the mean from the same pixel in a temporal window of one day before and one day after the day in question. After the temporal gap filling, the chosen functions (from Table 5) are applied to the AI and SZA data, and the results are reseasonalized by using Eq. 4 backwards.

3. **Smoothing and gap filling.** Possible gaps in the daily AOD maps are filled spatially using a 19×19 weighted-average matrix by location, which also smoothes the data. The weights equal 1/distance from the pixel to be filled.

4.2 AOD from TOMS-AI

1. **Resampling the data.** TOMS-AI has a different spatial resolution ($1^\circ \times 1^\circ$) than OMI. Hence, the TOMS-AI data are first resampled to the OMI resolution ($0.25^\circ \times 0.25^\circ$) and AI values above 4.5 are discarded.

2. **Missing data construction.** There is a gap in the TOMS data for 5/7/1993 – 7/21/1996. The missing data are constructed by calculating the mean value pixelwise from the same date in a temporal window of 3 years before and 3 years after the gap. Also, TOMS data have a calibration problem from 2000 onwards [26] which affects AI values. It is advised not to use AI data as a proxy of aerosol-related parameters. The change in the TOMS-AI data is most obvious from 2002 onwards, so we treat the period 2002–2004 as another gap of missing data. This temporal gap is filled the same way as the previous one.

3. **Deseasonalization.** The AI data are deseasonalized (the same way as described in step 1 in the Methods) with the deseasonalization coefficients calculated using the data from the years 1982–2004 excluding the constructed data from the temporal gaps.

4. **AOD calculation.** The possible gaps in the daily AI maps are filled. We try to fill the missing pixels using the mean from the same pixel in a temporal window of one day before and one day after the day in question. After the gap filling, the chosen functions (from Table 5) are applied to the AI and SZA data, and the results are reseasonalized by using Eq. 4 backwards.

5. **Smoothing and gap filling.** The constructed AOD maps have still large gaps in them that the weighted-average matrix cannot fill. The solution for this is to use monthly AOD climatology constructed from the OMI-AI (subsection 4.1). The gaps on the TOMS-AOD maps are filled using a spatial window of 9×9. Each window that has no data at all is filled from the climatology. This ensures that while using the weighted average matrix (23×23 matrix with 1/distance as weights) for minor gap filling and smoothing, in the border areas of climatology and calculated values, the latter ones also have a weight in the smoothing procedure, so that the climatology do not have a too dominant effect.

References

[1] Rahman, H. and Dedieu, G.: SMAC: a simplified method for the atmospheric correction of satellite measurements in the solar spectrum, International Journal of Remote Sensing, 15, 123–143, doi: 10.1080/01431169408954055, 1994

[2] Hsu, N. C.; Herman, J. R.; Torres, O.; Holben B. N.; Tanré, D.; Eck, T. F.; Smirnov, A.; Chatenet, B. and Lavenu, F.: Comparisons of the TOMS aerosol index with Sun-photometer aerosol optical thickness: Results and applications, Journal of Geophysical Research, 104(D6), 6269–6279, doi:10.1029/1998JD200086, 1999

[3] Torres, O.; Bhartia, P. K.; Herman, J. R.; Sinyuk,A.; Ginoux, P. and Holben, B.: A Long-Term Record of Aerosol Optical Depth from TOMS Observations and Comparison to AERONET Measurements. Journal of the Atmospheric Sciences, 59, 398–413, doi: 10.1175/1520-0469(2002)059<0398:ALTROA>2.0.CO;2, 2002

[4] Torres, O.; Bhartia, P. K.; Herman, J. R.; Ahmad, Z.; Gleason, J.: Derivation of aerosol properties from satellite measurements of backscattered ultraviolet radiation: Theoretical basis, Journal of Geophysical Research, vol 103, NO. D14, 17099–17110, doi: 10.1029/98JD00900, 1998

[5] de Graaf, M.; Stammes, P.; Torres, O. and Koelemeijer, R. B. A.: Absorbing Aerosol Index: Sensitivity analysis, application to GOME and comparison with TOMS, Journal of Geophysical Research, 110, D01201, doi:10.1029/2004JD005178, 2005

[6] Herman, J. R.; Bhartia, P. K.; Torres, O.; Hsu, C.; Seftor, C. and Celarier, E.: Global Distribution of UV-Absorbing Aerosols From Nimbus-7/TOMS Data, Journal of Geophysical Research, 102(D14), 16911–16922, doi: 10.1029/96JD03680, 1997

[7] TOMS Science Team: TOMS/Nimbus-7 Total Ozone Aerosol Index UV-Reflectivity UV-B Erythemal Irradiances Daily L3 Global 1 × 1.25 deg V008, Greenbelt, MD, Goddard Earth Sciences Data and Information Services Center (GES DISC), http://disc.sci.gsfc.nasa.gov/datacollection/TOMSN7L3_V008.html (accessed on 15 September 2017)

[8] TOMS Science Team: TOMS Earth-Probe Total Ozone (O3) Aerosol Index UV-Reflectivity UV-B Erythemal Irradiance Daily L3 Global 1 deg × 1.25 deg V008, Greenbelt, MD, Goddard Earth Sciences Data and Information Services Center (GES DISC), https://disc.gsfc.nasa.gov/datacollection/TOMSEPL3_008.html (accessed on 15 September 2017)

[9] McPeters, R. D.; Bhartia P. K.; Krueger, A. J.; Herman, Schlesinger, B. M.; Wellemeyer, C. G.; Seftor, C. J.; Jaros, G.; Taylor, S. L.; Swissler, T.; Torres, O.; Labow, G.; Byerly, W. and Cebula, R. P.: Nimbus-7 Total Ozone Mapping Spectrometer (TOMS) Data Products User's Guide, http://citeseerx.ist.psu.edu/viewdoc/download?doi=10.1.1.500.4152&rep=rep1&type=pdf (accessed on 15 September 2017), 1996

[10] McPeters, R. D.; Bhartia P. K.; Krueger, A. J.; Herman, J. R.; Wellemeyer, C. G.; Seftor, C. J.; Jaros, G.; Torres, O.; Moy, L.; Labow, G.; Byerly, W.; Taylor, S.L.; Swissler T. and Cebula, R.P.: Earth Probe Total Ozone Mapping Spectrometer (TOMS) Data Products User's Guide, http://ozoneaq.gsfc.nasa.gov/media/docs/epusrguide.pdf, (accessed on 15 September 2017) 1998

[11] OMI team: Ozone Monitoring Instrument (OMI),Data User's Guide, https://docserver.gesdisc.eosdis.nasa.gov/repository/Mission/OMI/3.3_ScienceDataProductDocumentation/3.3.2_ProductRequirements_Designs/README.OMI_DUG.pdf (accessed on 15 September 2017), 2002

[12] Stein-Zweers D. and Veefkind, P.: OMI/Aura Multi-wavelength Aerosol Optical Depth and Single Scattering Albedo L3 1 day Best Pixel in 0.25 degree × 0.25 degree V3, NASA Goddard Space Flight Center, Goddard Earth Sciences Data and Information Services Center (GES DISC), doi:10.5067/Aura/OMI/DATA3004 (accessed on 15 September 2017), 2012

[13] Hubanks, P.; Platnick, S.;, King, M. and Ridgway, B.: MODIS Atmosphere L3 Gridded Product Algorithm Theoretical Basis Document for C6, http://modis-atmos.gsfc.nasa.gov/_docs/L3_ATBD_C6.pdf (accessed on 15 September 2017), 2015

[14] Kaufman, Y. J.; Tanré, D.; Remer, L. A.; Vermote, E. F.; Chu, A. and Holben, B. N.: Operational remote sensing of tropospheric aerosol over land from EOS moderate resolution imaging spectroradiometer, Journal of Geophysical Research, 102(D14), 17051–17067, doi: 10.1029/96JD03988, 1997

[15] Remer, L. A.; Kaufman, Y. J.; Tanré, D.; Mattoo, S.; Chu, D. A.; Martins, J. V.; Li, R. R.; Ichoku, C.; Levy, R. C.; Kleidman, R. G.; Eck, T. F.; Vermote, E. and Holben, B. N.: The MODIS Aerosol Algorithm, Products, and Validation, Journal of the Atmospheric Sciences , 62: 947–973, doi:10.1175/JAS3385.1, 2005

[16] Levy, R. C.; Remer, L. A.; Mattoo, S.; Vermote, E. F. and Kaufman, Y. J.: Second-generation operational algorithm: Retrieval of aerosol properties over land from inversion of Moderate Resolution Imaging Spectroradiometer spectral reflectance, Journal of Geophysical Research, 112: 13211, doi: 10.1029/2006JD007811, 2007

[17] Levy, R. C.; Remer, L. A.; Kleidman, R. G.; Mattoo, S.; Ichoku, C.; Kahn, R.; and Eck, T. F.: Global evaluation of the Collection 5 MODIS dark-target aerosol products over land, Atmospheric Chemistry and Physics, 10, 10399–10420, 2010

[18] Hsu, N. C.; Tsay, S.; King, M. D. and Herman, J. R.: Aerosol Properties Over Bright-Reflecting Source Regions, IEEE Transactions on Geoscience and Remote Sensing, VOL 42, No.3, doi: 10.1109/TGRS.2004.824067, 2004

[19] Hsu, N. C.; Jeong, M-J; Bettenhausen, C.;, Sayer, A. M.; Hansell, R.; Seftor, C. S.; Huang, J. and Tsay, S.C.: Enhanced Deep Blue Aerosol Retrieval Algorithm: the 2nd Generation, Journal of Geophysical Research, doi: 10.1002/jgrd.50712, 2013

[20] Hansen, M.; DeFries, R.; Townshend, J. R. G.; and Sohlberg, R.: UMD Global Land Cover Classification, 1 Degree, 1.0, Department of Geography, University of Maryland, College Park, Maryland, 1981–1994, http://glcf.umd.edu/data/landcover/ (accessed on 15 September 2017), 1998

[21] European Commision, Joint Research Centre: The Global Land Cover Map for the Year 2000. GLC2000 database, http://forobs.jrc.ec.europa.eu/products/glc2000/products.php (accessed on 15 September 2017), 2003.

[22] Bhartia, P. K.: OMI/Aura TOMS-Like Ozone, Aerosol Index, Cloud Radiance Fraction L3 1 day 1 degree × 1 degree V3, NASA Goddard Space Flight Center, Goddard Earth Sciences Data and Information Services Center (GES DISC), doi:10.5067/Aura/OMI/DATA3001 (accessed on 15 September 2017)

[23] Torres, O.; Decae, R.; Veefkind, J. P. and de Leeuw, G.: OMI Aerosol Retrieval Algorithm, in OMI Algorithm Theoretical Basis Document: Clouds, Aerosols, and Surface UV Irradiance, Vol. 3, version 2, (OMI-ATBD-03, P. Stammes, Ed.), https://projects.knmi.nl/omi/documents/data/OMI_ATBD_Volume_3_V2.pdf (accessed on 15 September 2017), 2002

[24] Ångström, A. K.: On the atmospheric transmission of sun radiation and on the dust in the air, Geografiska Annaler, 12, 130–159, 1929

[25] Torres, O.; Tanskanen, A.; Veihelmann, B.; Ahn, C.; Braak, R.; Bhartia, P. K.; Veefkind, P. and Levelt, P.: Aerosols and surface UV products from Ozone Monitoring Instrument observations: An overview, Journal of Geophysical Research, 112, D24S47, doi:10.1029/2007JD008809, 2007

[26] Kiss, P.; Jánosi, I. M. and Torres, O.: Early calibration problems detected in TOMS Earth-Probe aerosol signal, Geophysical Research Letters, VOL. 34, L07803, doi:10.1029/2006GL028108, 2007

Table 1: Properties of the instruments, whose data we used for constructing the time series.

	Satellite	**Product**	**Version**	**Period**	**L3 resolution**
TOMS	Nimbus-7	TOMSN7L3	v8	11/1978 – 05/1993	$1.00^\circ \times 1.25^\circ$
TOMS	Earth Probe	TOMSEPL3	v8	07/1996 – 12/2005	$1.00^\circ \times 1.25^\circ$
OMI	Aura	OMAERO3	v003	08/2004 –	$0.25^\circ \times 0.25^\circ$
MODIS	Aqua	MYD08	005	05/2002 –	$1.00^\circ \times 1.00^\circ$
MODIS	Terra	MOD08	006	12/1999 –	$1.00^\circ \times 1.00^\circ$
AVHRR LUC	-	UMD Global Land Cover Classification	-	1981–1994	$1.00^\circ \times 1.00^\circ$
VEGETATION	SPOT 4	GLC 2000	-	2000	$0.01^\circ \times 0.01^\circ$

Table 2: Land use classification information.

Land use classification	**Subclass**	**Location or description**
1 Broadleaf evergreen forest	1	The Amazon and parts of Central America
	2	Congo river basin and Madagascar rainforests
	3	Rainforests of southeast Asia
2 Coniferous evergreen forest and woodland	4	North America taiga
	5	Eurasia taiga
3 High latitude deciduous forest and woodland	6	Transitional zone of North America taiga and tundra
	7	Transitional zone of Eurasia taiga and tundra
4 Tundra	8	North America tundra
	9	Eurasia tundra
5 Mixed coniferous forest and woodland	10	On the east coast of North America
	11	Central Europe
	12	Japan and small areas on the east coast of Asia
	13	Small areas in central Chile and in the northern Argentina
	14	Small areas in the southeast coast of Australia
	15	Small areas in the southern Africa
6 Wooded grassland	16	Parts of west coast of North America
	17	Areas in the southeast of USA and parts of Central America
	18	Areas on the north and northwest coast of South America
	19	Savanna area in the South America
	20	Southern Chile
	21	Parts of western Europe
	22	Savanna area below the Sahel in Africa
	23	Savanna area in the southern Africa
	24	Areas in the mainland southeast Asia
	25	Areas in the maritime southeast Asia
	26	southeast coast of Australia

Table 3: Land use classification information.

Land use classification		Subclass	Location or description
7	Grassland	27	Southern coast of Alaska
		28	South America prairies
		29	Small areas on the northern coast of South America
		30	On the southern part of the west coast of South America
		31	Areas in the northern and southern Argentina
		32	Southern Iceland and small areas in northern Europe
		33	Steppes of central Asia and western coast of India
		34	The Sahel
		35	Large areas in southern Africa (steppe area of southern Africa)
		36	Mostly the north coast of Australia, small areas in southern Australia
8	Bare ground	37	Small areas in western USA
		38	Southern coast of Peru and northern Chile
		39	The Sahara and the Middle East
		40	Gobi desert
		41	Namib desert
		42	Small area in central Australia
9	Shrubs and bare ground	43	Areas in western USA
		44	Most of southern Argentina, small parts of Chile and Peru
		45	Areas around the Sahara and parts in central Asia
		46	Kalahari desert
		47	Desert area in Australia

Table 4: Land use classification information.

Land use classification	Subclass	Location or description
10 Cultivated crops	48	Large area in central North America
	49	Small areas in Mexico and in the southern part of Central America
	50	Small areas along the east coast of South America
	51	Most of central Europa
	52	Small areas around the Sahel and small areas in southern Africa
	53	Eastern China
	54	Most of India
	55	Small areas in mainland and maritime Southeast Asia
	56	Areas around the desert area in Australia
11 Broadleaf deciduous forest and woodland	57	Small areas in western North America
	58	Small areas in eastern North America
	59	Small areas in the middle of South America
	60	Small areas in central Europe
	61	Small areas in southern Africa
	62	Small areas on east coast of Russia
	63	Small areas in mainland Southeast Asia
	64	Small areas in maritime Southeast Asia and in Australia
- -	65	New Zealand

Table 5: Information of the best-fitting functions chosen for each subclass. α is the linear and β the constant regression coefficient. *D* stands for which deseasonalization method (mean or median) is used and *r* stands for the correlation coefficient of the regression.

Area	α	β	*D*	*r*	Area	α	β	*D*	*r*
1	0.325	0.339	median	0.5	34	0.166	0.190	mean	0.6
2	0.209	0.264	median	0.5	35	0.261	0.096	mean	0.5
3	0.307	0.217	median	0.5	36	0.095	0.052	median	0.5
4	0.367	0.088	median	0.5	37	0.135	0.197	mean	0.5
5	0.313	0.110	median	0.6	38	0.044	0.210	median	0.5
6	0.102	0.515	mean	0.7	39	0.189	0.119	mean	0.5
7	0.578	0.109	median	0.5	40	0.249	0.156	median	0.5
8	0.112	0.125	median	0.5	41	0.127	0.119	mean	0.6
9	0.208	0.095	median	0.5	42	0.060	0.088	mean	0.7
10	0.047	0.133	mean	0.5	43	0.144	0.126	mean	0.8
11	0.081	0.160	mean	0.5	44	0.048	0.145	median	0.5
12	0.164	0.328	mean	0.6	45	0.183	0.176	mean	0.6
13	0.126	0.214	mean	0.5	46	0.157	0.098	median	0.5
14	0.144	0.084	mean	0.5	47	0.038	0.079	mean	0.8
15	0.317	0.089	mean	0.8	48	0.130	0.138	mean	0.5
16	0.186	0.113	mean	0.5	49	0.099	0.141	mean	0.8
17	0.034	0.134	mean	0.7	50	0.105	0.110	mean	0.5
18	0.168	0.254	mean	0.5	51	0.151	0.163	mean	0.5
19	0.212	0.140	median	0.5	52	0.202	0.198	mean	0.5
20	-0.015	0.068	median	0.8	53	0.458	0.297	median	0.5
21	0.161	0.141	mean	0.5	54	0.173	0.298	mean	0.7
22	0.247	0.131	median	0.5	55	0.066	0.313	median	0.7
23	0.356	0.113	mean	0.8	56	0.085	0.081	mean	0.5
24	0.287	0.215	mean	0.8	57	0.049	0.145	mean	0.8
25	0.092	0.138	median	0.5	58	0.092	0.139	mean	0.6
26	0.106	0.080	mean	0.5	59	0.182	0.222	median	0.5
27	-0.187	0.199	median	0.5	60	0.197	0.146	mean	0.7
28	0.110	0.136	mean	0.5	61	0.210	0.179	mean	0.6
29	0.118	0.268	mean	0.5	62	0.112	0.319	mean	0.8
30	0.061	0.445	median	0.7	63	0.170	0.317	mean	0.5
31	0.063	0.113	median	0.7	64	0.087	0.101	mean	0.5
32	0.089	0.111	mean	0.5	65	0.021	0.052	median	0.5
33	0.205	0.160	mean	0.8	-	-	-	-	-

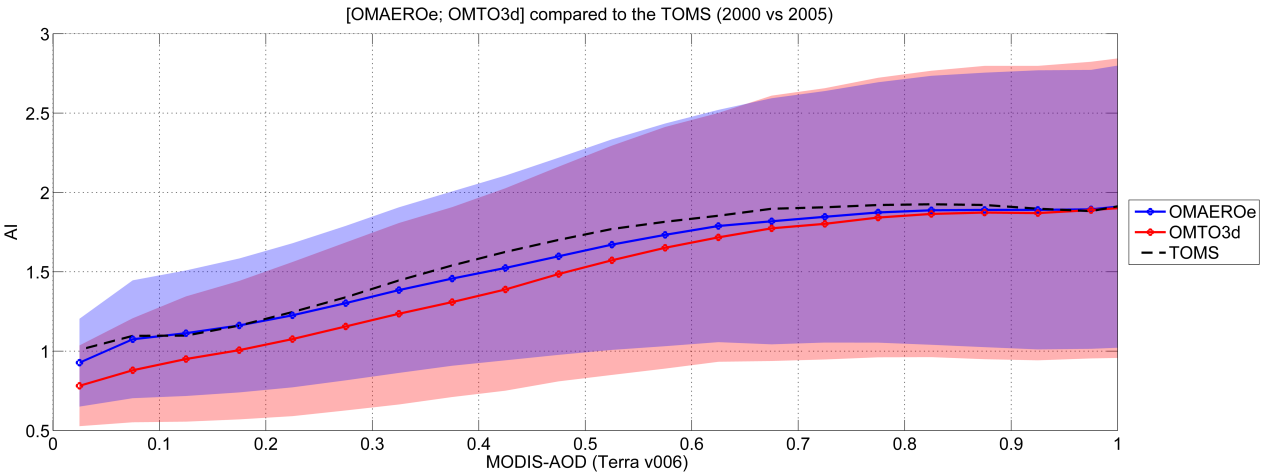

Figure 1: Global comparison between Terra MODIS-AOD and TOMS-AI from the year 2000 (black), and comparison between Terra MODIS-AOD and AI data from OMAERROe (blue) and OMTO3d (red) from the year 2005. The upper limit of the reddish (blueish) area behind the curves indicates the mean of OMAERROe-AI (OMTO3d-AI) values with added standard deviation and the lower limit indicates the mean of OMAERROe-AI (OMTO3d-AI) values with subtracted standard deviation.

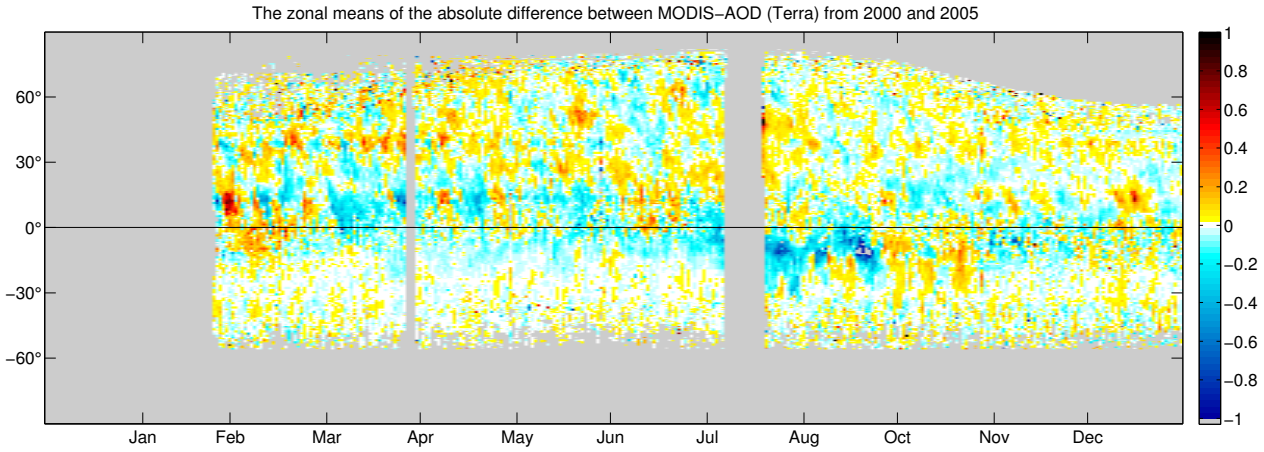

Figure 2: Zonal means of the absolute differences over land between MODIS-AOD data (Terra) from years 2000 and 2005.

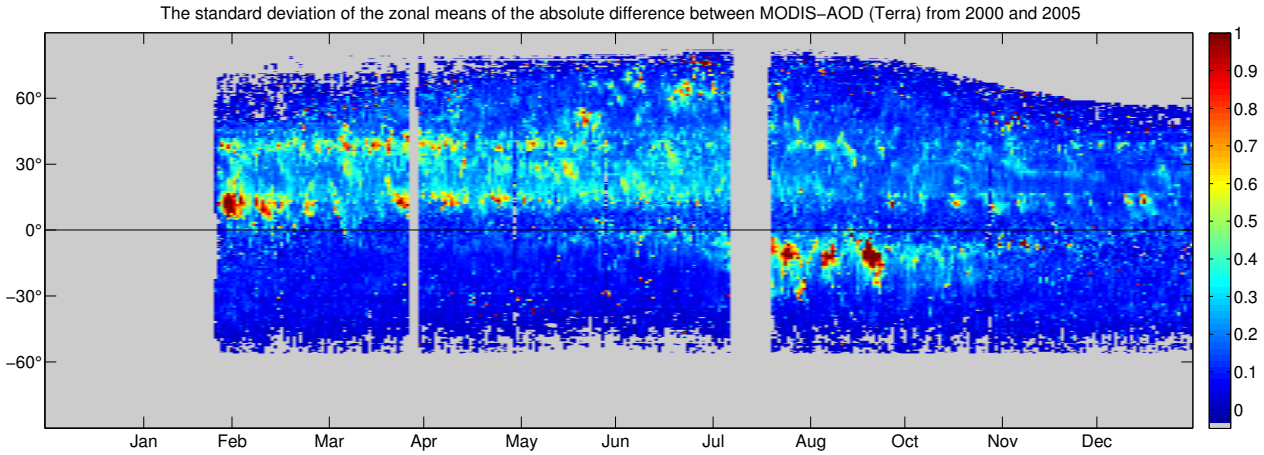

Figure 3: Standard deviation of zonal means of the absolute differences over land between MODIS-AOD data (Terra) from years 2000 and 2005.

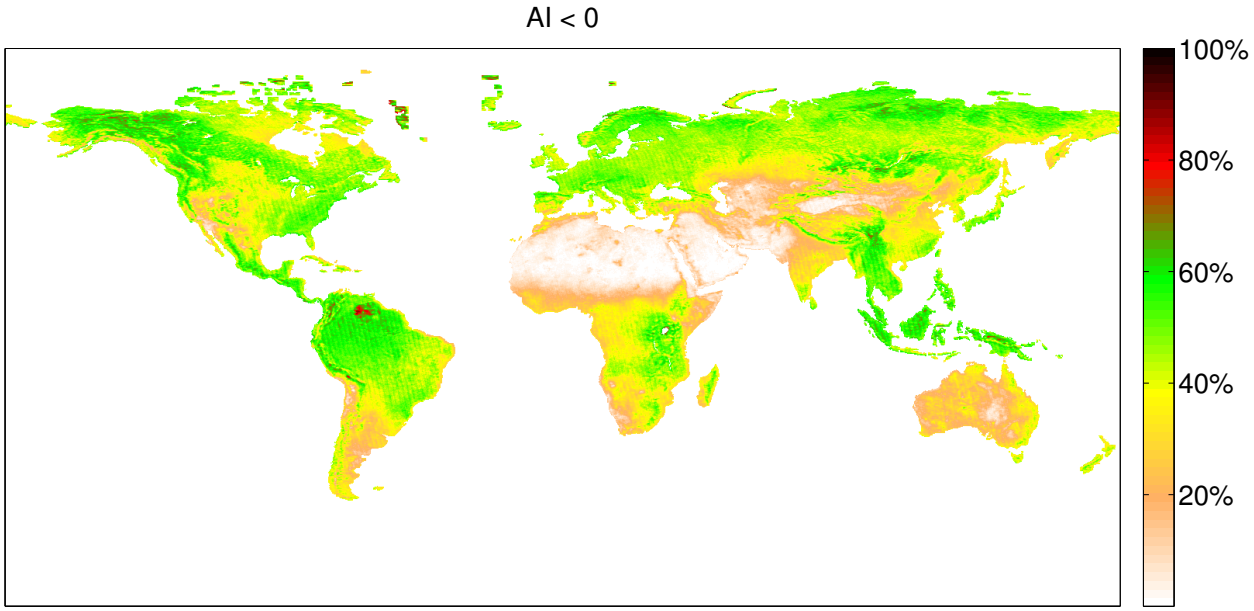

Figure 4: The percentage of negative AI values globally in the year 2008.

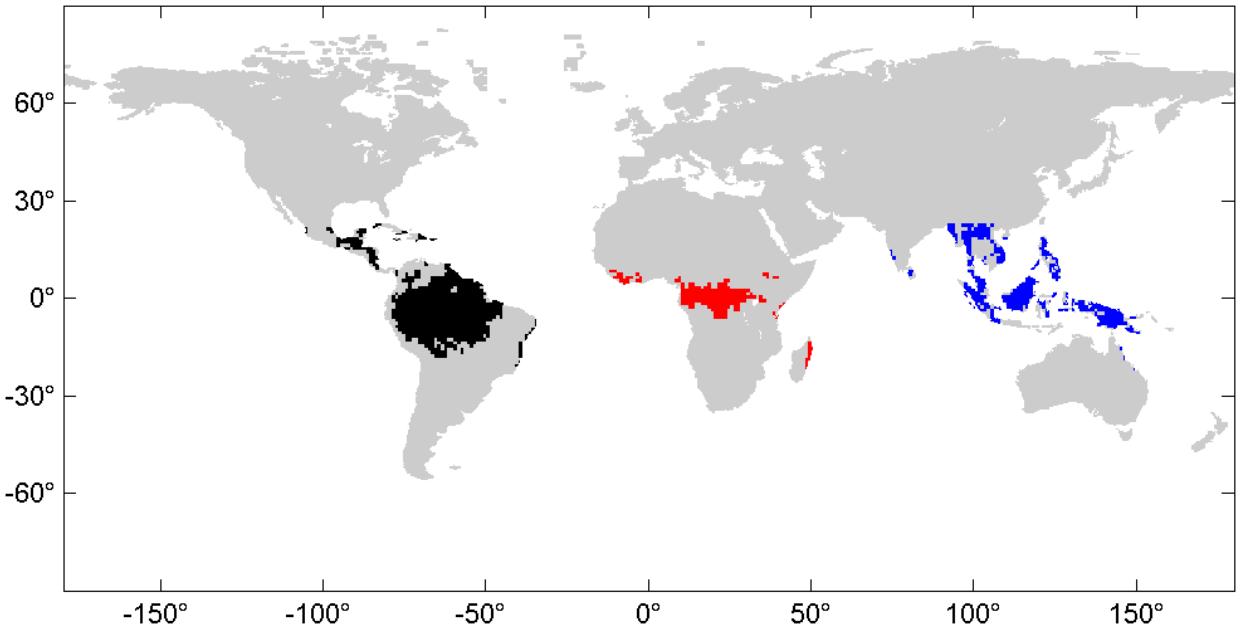

Figure 5: An example of data division using AVHRR-LUC data. Coloured areas (black, red and blue) all have land use classification value 1 (Broadleaf evergreen forest). Based on the location, class 1 is divided into 3 subclasses (marked by the different colours), which are treated separately when processing the AOD time series (Tables 2 – 4).

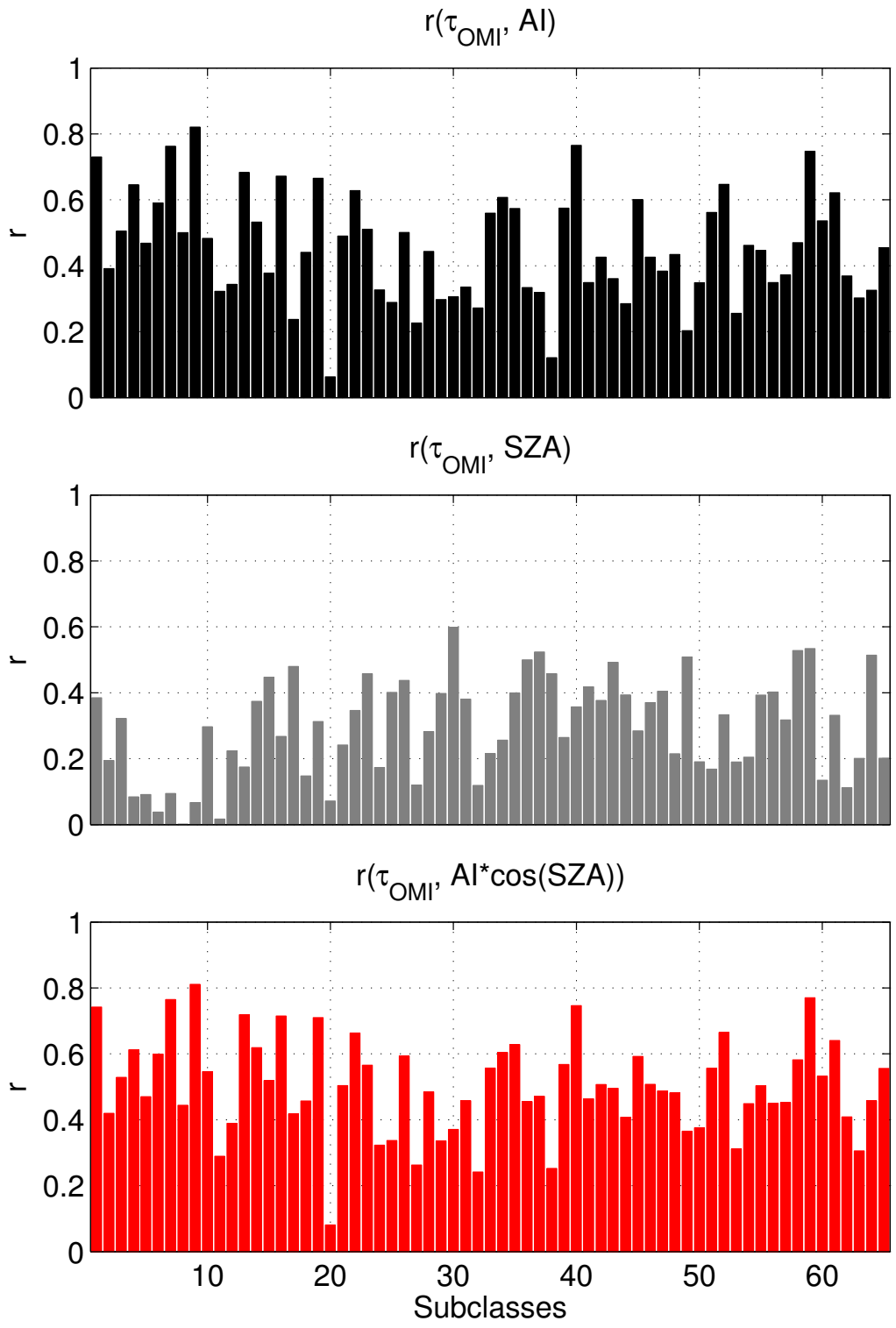

Figure 6: The correlation coefficients of AOD and AI (topmost), of AOD and SZA (middle) and of AOD and AI data multiplied with cos(SZA) (bottom) of different subclasses for the years 2005–2008.

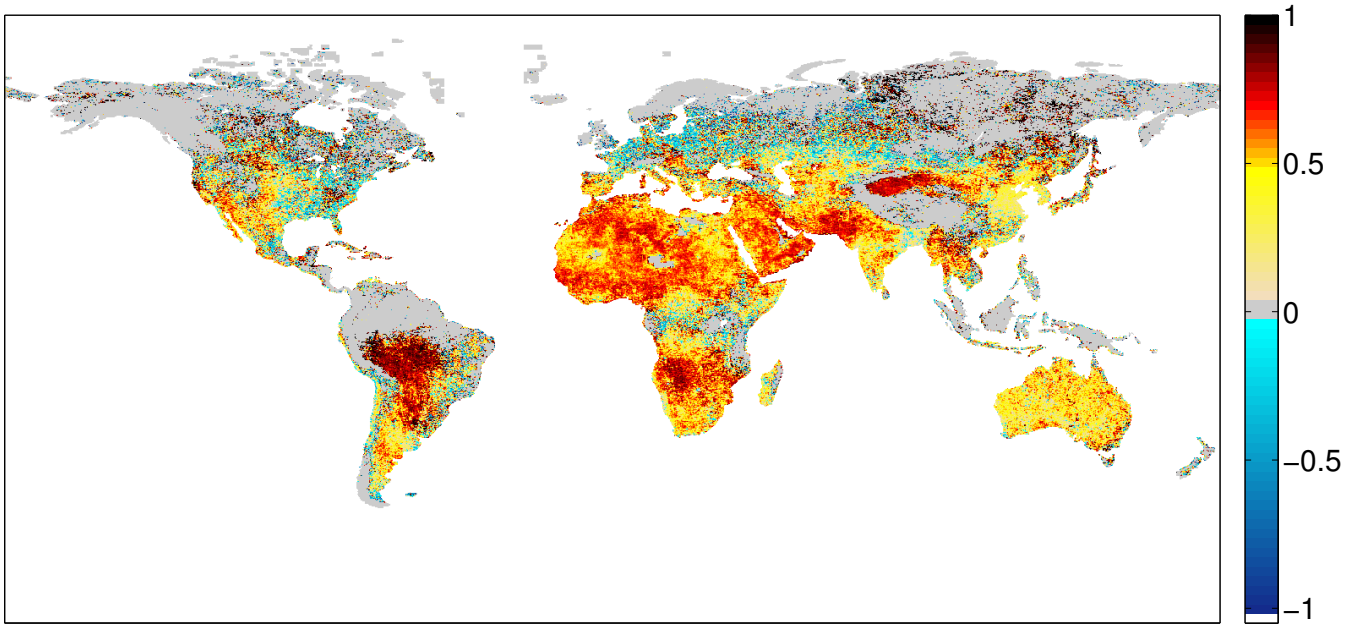

Figure 7: The correlation coefficients of AOD and AI·cos(SZA) pixelwise for the years 2005–2008. The grey colour indicates the area without data.

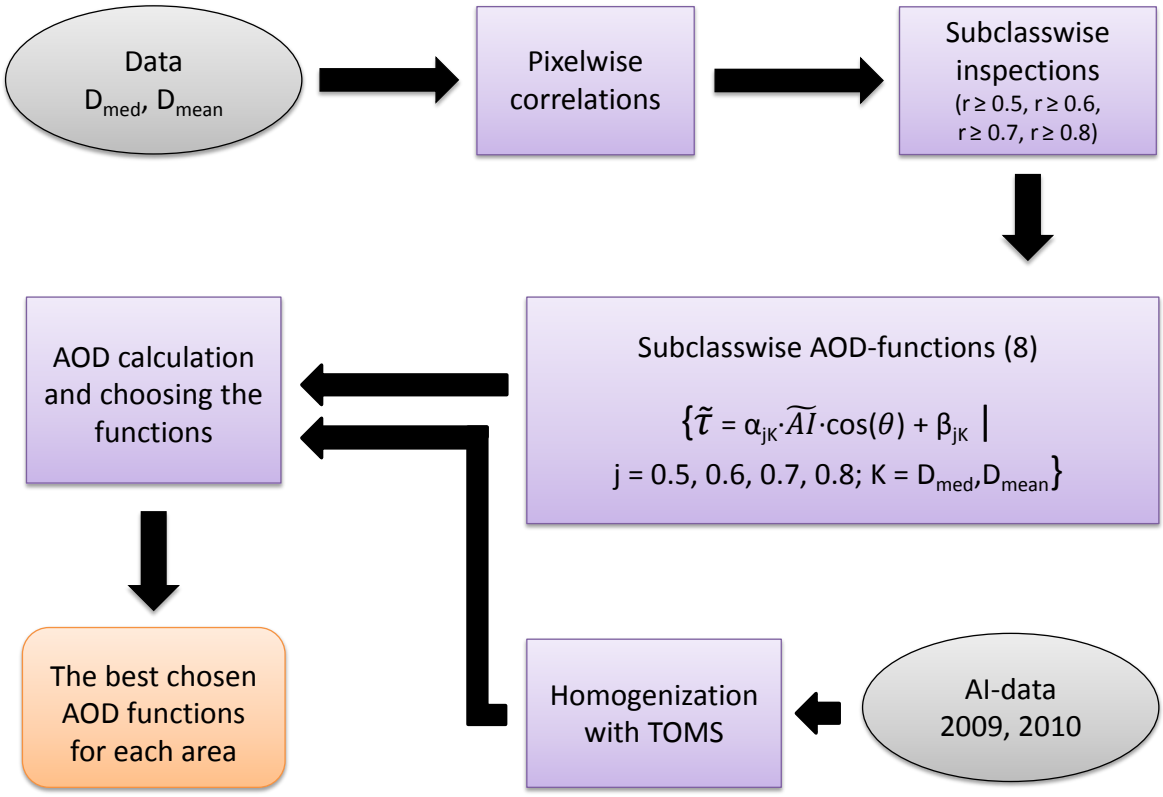

Figure 8: Flowchart of the process of choosing the best functions.

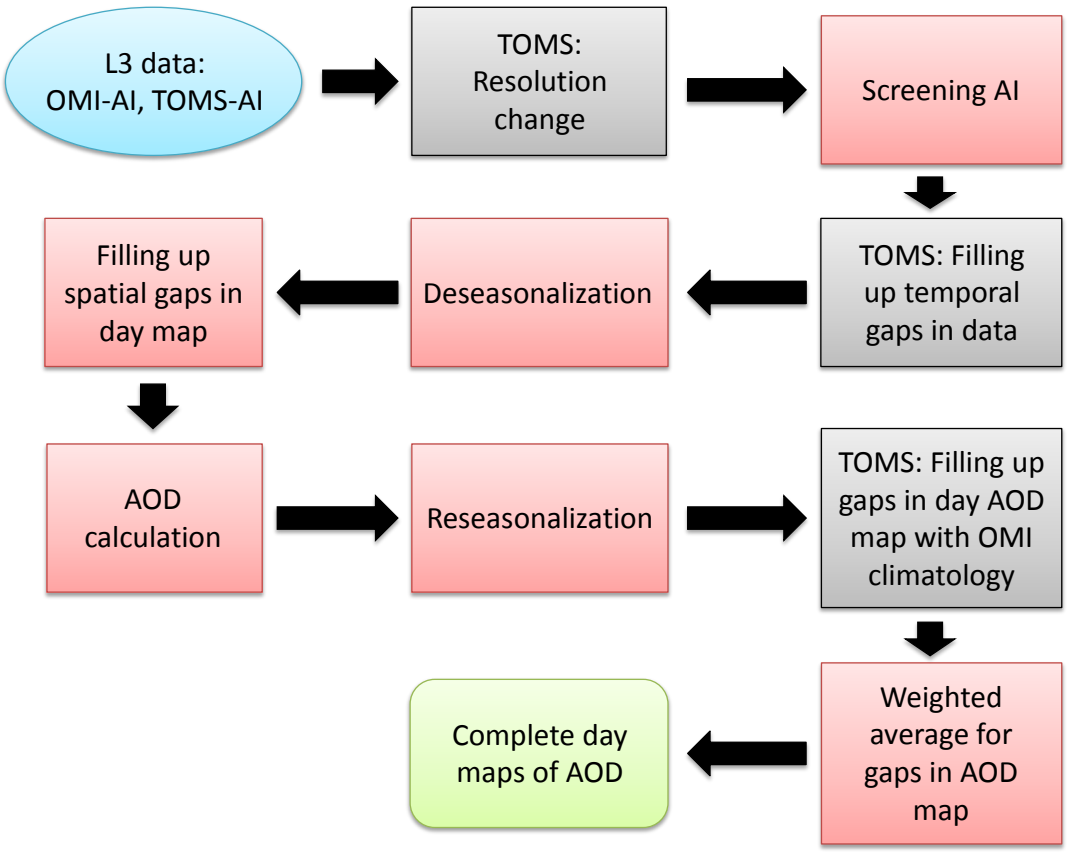

Figure 9: Flowchart of the process of calculating the AOD maps using OMI-AI, TOMS-AI and SZA information. Steps marked with red are applied to both data sets, while those marked with grey are applied only to TOMS.

ILMATIETEEN LAITOS
METEOROLOGISKA INSTITUTET
FINNISH METEOROLOGICAL INSTITUTE

FINNISH METEOROLOGICAL INSTITUTE
Erik Palménin aukio 1
00560 Helsinki
tel. +358 29 539 1000
WWW.FMI.FI

FINNISH METEOROLOGICAL INSTIUTE
RAPORTS 2017:2
ISBN 978-952-336-013-6 (pdf)
ISSN 0782-6079
Helsinki 2017